Results in Physics 8 (2018) 610–620

Contents lists available at ScienceDirect

Results in Physics

journal homepage: www.journals.elsevier.com/results-in-physics

Effects of heat and mass transfer on unsteady boundary layer flow of a chemical reacting Casson fluid

Kashif Ali Khan [a,*], Asma Rashid Butt [a], Nauman Raza [b]

[a] Department of Mathematics, University of Engineering and Technology, Lahore, Pakistan
[b] Department of Mathematics, University of the Punjab, Lahore, Pakistan

ARTICLE INFO

Article history:
Received 23 October 2017
Received in revised form 22 December 2017
Accepted 30 December 2017
Available online 4 January 2018

Keywords:
HAM
Casson fluid
Stretching sheet
Similarity transform
Heat source
Chemical reaction

ABSTRACT

In this study, an endeavor is to observe the unsteady two-dimensional boundary layer flow with heat and mass transfer behavior of Casson fluid past a stretching sheet in presence of wall mass transfer by ignoring the effects of viscous dissipation. Chemical reaction of linear order is also invoked here. Similarity transformation have been applied to reduce the governing equations of momentum, energy and mass into non-linear ordinary differential equations; then Homotopy analysis method (HAM) is applied to solve these equations. Numerical work is done carefully with a well-known software MATHEMATICA for the examination of non-dimensional velocity, temperature, and concentration profiles, and then results are presented graphically. The skin friction (viscous drag), local Nusselt number (rate of heat transfer) and Sherwood number (rate of mass transfer) are discussed and presented in tabular form for several factors which are monitoring the flow model.

Introduction

The study of heat and mass transfer effects has a lot of applications in engineering especially in industry and manufacturing processes. For example, extrusion of polymers, copper wires drawing, continuous metals casting, glass-fiber production, human transpiration, atomic power plants, cooling of electronic equipment, filtration, refrigeration, spreading of chemical pollutants in plants, injection and diffusion of medicine in blood veins and crude oil's purification. The fluid whose properties cannot be explained by Newtonian fluid models is called a non-Newtonian fluid. Blood cells is a type of non-Newtonian fluid and can be considered as Casson fluid due to the chain structure of blood cells and the substances like fibrinogen, rouleaux, protein etc. There are many other important and strong applications of Casson fluids for example, in industry; fluids behave like elastic solids and for such fluids, a yield shear stress exists in the constitutive equations. Recently time dependent/independent boundary layer models of Casson fluid has attained phenomenal attention due to its rheological applications especially in chemical and mechanical engineering. Researchers, numerical analyst and engineers which are attached with that area of research are putting their efforts to solve these complex Casson fluid models [1–8]. A stretched medium is a kind of sheet that deals with the ambient fluid both thermally and mechanically during a manufacturing process. That's the reason, the fluid flow behavior past that surface, which involves in finding the rate of cooling, has great importance in industrial, manufacturing and technological processes like polymer films or thin sheets production [9–11]. Crane [12] was the first who work on the fluid's flow of stretching sheet of linear order in 1970 and find the similarity solution of the steady-problem. Chiam [13,14] also work on stagnation point flow past a stretching sheet in 1994 where velocity of stretching sheet is equal to the straining velocity of stagnation point flow, then extended the idea to heat transfer with variable conductivity past a stretching sheet in 1996. Some of the research work related to stagnation point flow over a stretching/shrinking sheet to above one is mentioned in [15–23].

Due to amicable applications of stretching plates and a non-Newtonian fluid like Casson fluid, attracts many scientist and researchers. K Bhattacharyya do work by adding heat transfer and magnetic effects in the model of Casson fluid past a stretching sheet [24]. Already dual solution in boundary layer flow with mass transfer analysis have been obtained by Bhattacharyya et al. [25] and extended it to obtaining the analytic solutions of MHD Casson fluid flow over stretching/shrinking sheet with suction or injection effects [26]. Shehzad and Hayat [27] find the series solution after analyzing the non-linear steady model under mass transfer effects on MHD Casson fluid model with chain reaction and suction effects; where similar effects are seen under the influence of

* Corresponding author.
E-mail address: kashifali@uet.edu.pk (K.A. Khan).

https://doi.org/10.1016/j.rinp.2017.12.080
2211-3797/

Nomenclature

u	axial velocity part along x-axis	D	diffusion coefficient
v	transverse velocity part along y-axis	ψ	physical stream function
x	horizontal coordinate	β	Casson parameter
y	vertical coordinate	a	straining rate parameter
ρ	density of fluid	b	stretching rate parameter
υ	kinematic viscosity	γ	velocity ratio parameter
μ	dynamic viscosity	η	similarity variable
μ_D	plastic dynamic viscosity	ϑ	dimensionless stream function
Y_δ	fluid's yield stress	A	unsteady parameter
U_w	velocity of the stretching surface	ϑ	dimensionless temperature
V_w	wall mass suction/injection	Φ	dimensionless concentration
U_∞	straining velocity	f_0	wall mass transfer parameter
τ	temperature of the field	β^*	reaction rate parameter
$\mathbb{C}$	species concentration	S_C	Schmidt number
τ_w	temperature near to sheet	Pr	Prandtl number
τ_∞	temperature away from sheet	C_f	Skin friction coefficient
$\mathbb{C}_w$	constant concentration	N_u	Nusselt number
$\mathbb{C}_\infty$	concentration in free stream	S_h	Sherwood number
R	reaction rate of solute		

magnetic and Casson parameter on the velocity profile. Sandeep [28] present work with the collaboration of other researchers in finding the analytical solutions of Casson fluid flow past a stretchy sheet which is permeable and exponentially long where dual results are obtained and shows the comparison between Newtonian and Casson fluid. Recently, Bilal and Hayat [29] worked on steady model of MHD mixed convection Casson fluid flow with the involvement of Hall and thermal diffusion effects past a stretching sheet. Most of the models of Casson fluid models in heat and mass transfer analysis are steady. Unsteady models of non-Newtonian fluids past a stretching sheet have gained less attentions. However, the unsteady flow models with irregular domains are also under interest as Dehghan [30] work on time dependent incompressible Navier-Stokes equations by introducing some new numerical techniques. Recently, he [31,32] shows tremendous work in boundary layer problems containing irregular domain and provides the numerical plan for 2D Rayleigh-Stokes model with fractional derivative. Also, Tsai [33] give the solutions of highly nonlinear partial differential equations with irregular domain by using hybrid homotopy technique (HAM; homotopy analysis method + MFS; method of fundamental solutions + APS; Augmented polynomial spline). In present work, HAM is provoked to get the solution of an unsteady Casson fluid model over simple domain past a stretching sheet with heat, mass transfer along 1st order chemical reaction.

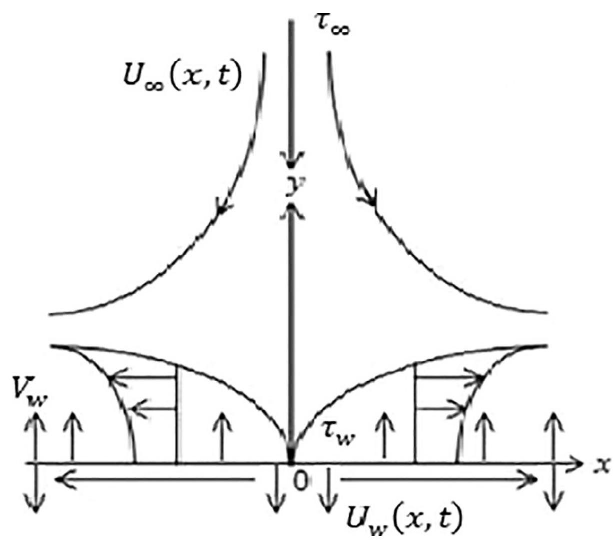

Fig. 1. Flow Model.

Flow analysis

Consider the unsteady two-dimensional stagnation point flow of a non-Newtonian Casson fluid over a stretching sheet. The fluid flow is restricted to $y > 0$ with the involvement of 1st order chemical reaction. Fig. 1 tells that flow is modelled by stretching of a bounding and non-conducting sheet. The wall is stretched by applying two equal and opposite forces along the x-axis, keeping the origin fixed in such a way that the rate of movement of the sheet is of 1st order in that flow regime. For an isotropic and incompressible Casson fluid flow, the rheological equation of state can be stated as (see [34])

$$\tau_{ij} = \begin{cases} \left(2\mu_D + Y_\delta\sqrt{\frac{2}{\pi}}\right)e_{ij}, & \pi > \pi_p \\ \left(2\mu_D + Y_\delta\sqrt{\frac{2}{\pi_p}}\right)e_{ij}, & \pi < \pi_p \end{cases}$$

where μ_D is the plastic dynamic viscosity, Y_δ is the fluid's yield stress, $\pi = e_{ij}e_{ij}$ is the multiplication of the component of deformation rate with itself, e_{ij} is the $(i,j)^{th}$ component of the deformation rate and π_p is the critical value of this product based on that model. The governing equations for above flow model are (see details [35]):

$$\frac{\partial u}{\partial x} + \frac{\partial v}{\partial y} = 0 \tag{1}$$

$$\frac{\partial u}{\partial t} + u\frac{\partial u}{\partial x} + v\frac{\partial u}{\partial y} = \frac{\partial U_\infty}{\partial t} + U_\infty\frac{\partial U_\infty}{\partial x} + \nu\left(1 + \frac{1}{\beta}\right)\frac{\partial^2 u}{\partial y^2} \tag{2}$$

$$\frac{\partial \tau}{\partial t} + u\frac{\partial \tau}{\partial x} + v\frac{\partial \tau}{\partial y} = \alpha\frac{\partial^2 \tau}{\partial y^2} \tag{3}$$

$$\frac{\partial \mathbb{C}}{\partial t} + u\frac{\partial \mathbb{C}}{\partial x} + v\frac{\partial \mathbb{C}}{\partial y} = D\frac{\partial^2 \mathbb{C}}{\partial y^2} - R(\mathbb{C} - \mathbb{C}_\infty) \tag{4}$$

Then the suitable initial and boundary conditions are given by:

$$\left.\begin{aligned} At\ t = 0, u(x,y,0) = bx, v(x,y,0) = -\sqrt{av}f_0, \\ \tau(x,y,0) = \tau_\infty + cx, \mathbb{C}(x,y,0) = \mathbb{C}_w \\ At\ y = 0, u = U_w(x,t), v = V_w(t), \tau = \tau_w, C = \mathbb{C}_w \\ As\ y \to \infty, u \to U_\infty(x), \tau \to \tau_\infty, C \to \mathbb{C}_\infty \\ U_w(x,t) = bx(1-\lambda t)^{-1}, U_\infty(x,t) = ax(1-\lambda t)^{-1} \\ \tau_w(x,t) - \tau_\infty = cx(1-\lambda t)^{-1} \end{aligned}\right\} \tag{5}$$

where u, v are the components of velocity along x, y directions, ρ is the density, v is the kinematic viscosity,α is the thermal diffusivity, D is the mass diffusivity, R is the reaction rate, $U_w(x,t)$ is the stretching velocity of sheet (where b > 0 is the stretching parameter/constant), $U_\infty(x,t)$ is the free stream velocity or velocity of external flow (i.e. in the absence of pressure gradient); a > 0 is the strength of stagnation flow. τ is the thermal reading of the sheet, τ_∞ is the thermal reading of the fluid far away from the sheet, $\tau_w(x,t)$ is the surface temperature with c is any constant, $\mathbb{C}$the strength/concentration of the substance and $\mathbb{C}_w$ is the constant concentration at the stretching sheet, $\mathbb{C}_\infty$is also the fixed concentration but in free stream.

Eq. (1) is identically satisfied after involving the stream function $\psi(x,y,t)$ as

$$u = \frac{\partial\psi(x,y,t)}{\partial y}, v = -\frac{\partial\psi(x,y,t)}{\partial x} \tag{6}$$

To find similarity solutions, we will solve the above equations by using suitable similarity transformation discussed in [36] as follows.

$$\psi(x,y,t) = \sqrt{\frac{av}{(1-\lambda t)}}x\mathfrak{f}(\eta),\ \ \eta(y,t) = \sqrt{\frac{a}{v(1-\lambda t)}}y,$$
$$\theta(\eta) = \frac{\tau - \tau_\infty}{\tau_w - \tau_\infty},\ \ \Phi(\eta) = \frac{\mathbb{C} - \mathbb{C}_\infty}{\mathbb{C}_w - \mathbb{C}_\infty} \tag{7}$$

where η is the similarity variable. Therefore, the mass transfer velocity can be of the type $V_w(t) = -\sqrt{\frac{av}{(1-\lambda t)}}f_0$. Now the modified form boundary value problem is

$$\left(1+\frac{1}{\beta}\right)\mathfrak{f}^{(3)} + \mathfrak{f}\mathfrak{f}^{(2)} - \left(\mathfrak{f}^{(1)}\right)^2 - A(\mathfrak{f}^{(1)} + \frac{\eta}{2}\mathfrak{f}^{(2)}) + (1+A) = 0 \tag{8}$$

$$\vartheta^{(2)} + \Pr\{\mathfrak{f}\vartheta^{(1)} - \mathfrak{f}^{(1)}\vartheta - A(\vartheta + \frac{\eta}{2}\vartheta^{(1)})\} = 0 \tag{9}$$

$$\Phi^{(2)} + Sc\{\mathfrak{f}\Phi^{(1)} - A\frac{\eta}{2}\Phi^{(1)} - \beta^*\Phi\} = 0 \tag{10}$$

with boundary conditions

$$\left.\begin{aligned} At\ \eta = 0, \mathfrak{f}(0) = f_0, \mathfrak{f}^{(1)}(0) = \gamma, \vartheta(0) = 1, \Phi(0) = 1 \\ As\ \eta \to \infty, \mathfrak{f}^{(1)}(\infty) \to 1, \vartheta(\infty) \to 0, \Phi(\infty) \to 0 \end{aligned}\right\} \tag{11}$$

where $\beta = \mu_D\frac{\sqrt{2\pi_p}}{Y_\delta}, \beta^* = \frac{R}{a}, Sc = \frac{v}{D}, Pr = \frac{v}{\alpha}, A = \frac{\lambda}{a}, \gamma = \frac{b}{a}$represent the Casson fluid factor, reaction rate factor, Schmidt number, Prandtl number, unsteadiness factor and velocity ratio parameter. The wall mass transfer parameter is f_0 where $f_0 > 0$, $f_0 < 0$ used for wall mass suction, injection parameter. $\mathfrak{f}^{(1)}$is the notation of derivative with respect to η. Skin friction coefficient $C_\mathfrak{f}$, local rate of heat transfer coefficient N_u and local Sherwood number S_h which are the physical quantities of interest, defined as follows

$$C_\mathfrak{f} = \frac{2\tau_w}{\rho U^2},\ \ N_u = \frac{xq_w}{k(\tau_w - \tau_\infty)},\ \ S_h = \frac{xh_m}{D(\mathbb{C}_w - \mathbb{C}_\infty)} \tag{12}$$

The wall shear stress, heat flux and mass flux are defined as

$$\tau_w = \mu\frac{\partial u}{\partial y}\bigg|_{y=0},\ \ q_w = -k\frac{\partial\tau}{\partial y}\bigg|_{y=0},\ \ q_w = -D\frac{\partial\mathbb{C}}{\partial y}\bigg|_{y=0} \tag{13}$$

Now using the similarity variables Eq. (7), we get

$$\frac{1}{2}C_\mathfrak{f}\sqrt{Re_x} = (1+\frac{1}{\beta})\mathfrak{f}''(0),\ \ \frac{N_u}{\sqrt{Re_x}} = -\vartheta'(0), \frac{S_h}{\sqrt{Re_x}} = -\Phi'(0) \tag{14}$$

Now, we have to find the analytic-numeric solution of boundary value problem (8)–(11).

Solution by HAM

The solution of the above governing nonlinear equations (8)–(10) is obtained after applying the homotopy analysis method (HAM) inspired by the Pioneer of that method [37]. According to the boundary conditions of (11), the suitable initial guesses for velocity, temperature and concentration profile by using the first rule of solution expression are given below as

$$\mathfrak{f}_0(\eta) = (1-\gamma)(\exp(-\eta) - 1) + \eta + f_0,$$
$$\vartheta_0(\eta) = \exp(-\eta), \Phi_0(\eta) = \exp(-\eta) \tag{15}$$

and

$$\mathcal{L}(\mathfrak{f}) = \frac{\partial^3\mathfrak{f}}{\partial\eta^3\mathfrak{f}} + \frac{\partial^2}{\partial\eta^2},\ \ \mathcal{L}(\vartheta) = \frac{\partial^2\vartheta}{\partial\eta^2} + \frac{\partial\vartheta}{\partial\eta},\ \ \mathcal{L}(\Phi) = \frac{\partial^2\Phi}{\partial\eta^2} + \frac{\partial\Phi}{\partial\eta} \tag{16}$$

are the auxiliary linear operators satisfying the properties

$$\begin{cases} \mathcal{L}[d_1 + d_2\eta + d_3e^{-\eta}] = 0 \\ \mathcal{L}[d_4e^{\eta} + d_5e^{-\eta}] = 0 \\ \mathcal{L}[d_6e^{\eta} + d_7e^{-\eta}] = 0 \end{cases} \tag{17}$$

where $d_j(j = 1,2,\ldots,7)$ are the constants.

3.1 Zeroth order deformation problem

$$(1-\mathbf{r})\mathcal{L}[\hat{\mathfrak{f}}(\eta,r) - \mathfrak{f}_0(\eta)] = r\hbar_\mathfrak{f}\mathcal{H}(\eta)\mathcal{N}[\hat{\mathfrak{f}}(\eta,r)] \tag{18}$$

$$(1-\mathbf{r})\mathcal{L}[\hat{\vartheta}(\eta,r) - \vartheta_0(\eta)] = r\hbar_\vartheta\mathcal{H}^*(\eta)\mathcal{N}[\hat{\vartheta}(\eta,r)] \tag{19}$$

$$(1-\mathbf{r})\mathcal{L}[\hat{\Phi}(\eta,r) - \Phi_0(\eta)] = r\hbar_\Phi\mathcal{H}^\#(\eta)\mathcal{N}[\hat{\Phi}(\eta,r)] \tag{20}$$

subject to conditions

$$\hat{\mathfrak{f}}(0,r) = f_0, \hat{\mathfrak{f}}^{(1)}(0,r) = \gamma, \hat{\mathfrak{f}}^{(1)}(\infty,r) = 1, \hat{\vartheta}(0,r) = 1,$$
$$\hat{\vartheta}(\infty,r) = 0, \hat{\Phi}(0,r) = 1, \hat{\Phi}(\infty,r) = 0 \tag{21}$$

In Eq. (21), boundary conditions be adjusted after the existence of embedding parameter where $0 \leqslant r \leqslant 1$ due to the inherited property of HAM [For details; see references [38–40]].

$$\mathcal{N}[\hat{\mathfrak{f}}(\eta,r)] = \left(1+\frac{1}{\beta}\right)\frac{\partial^3\mathfrak{f}(\eta,r)}{\partial\eta^3} + f(\eta,r)\frac{\partial^2\mathfrak{f}(\eta,r)}{\partial\eta^2} - \left(\frac{\partial\mathfrak{f}(\eta,r)}{\partial\eta}\right)^2 A\left(\frac{\partial\mathfrak{f}(\eta,r)}{\partial\eta} + \frac{\eta}{2}\frac{\partial^2\mathfrak{f}(\eta,r)}{\partial\eta^2}\right) + (1+A) \tag{22}$$

$$\mathcal{N}[\hat{\vartheta}(\eta,r)] = \frac{\partial^2\vartheta(\eta,r)}{\partial\eta^2} + \Pr\left\{\not{f}(\eta,r)\frac{\partial\vartheta(\eta,r)}{\partial\eta} - \vartheta(\eta,r)\frac{\partial\not{f}(\eta,r)}{\partial\eta}A\left(\vartheta(\eta,r) + \frac{\eta}{2}\frac{\partial\vartheta(\eta,r)}{\partial\eta}\right)\right\} \tag{23}$$

$$\mathcal{N}[\hat{\Phi}(\eta,r)] = \frac{\partial^2\Phi(\eta,r)}{\partial\eta^2} + S_c\left\{\not{f}(\eta,r)\frac{\partial\Phi(\eta,r)}{\partial\eta} - A\frac{\eta}{2}\frac{\partial\Phi(\eta,r)}{\partial\eta} - \beta^*\Phi(\eta,r)\right\} \tag{24}$$

having non-linear operators. $\hbar_{\mathfrak{f}}, \hbar_{\vartheta}, \hbar_{\Phi}$ the convergence control parameters and

$$\mathcal{H}(\eta) = \exp(-\eta), \mathcal{H}^*(\eta) = \exp(-\eta), \mathcal{H}^{\#}(\eta) = \exp(-\eta) \tag{25}$$

are the auxiliary non-zero functions. For $r = 0$ and $r = 1$, we get

$$\hat{\mathfrak{f}}(\eta,0) = \mathfrak{f}_0(\eta), \hat{\vartheta}(\eta,0) = \vartheta_0(\eta), \hat{\Phi}(\eta,0) = \Phi_0(\eta) \tag{26}$$

$$\hat{\mathfrak{f}}(\eta,1) = \mathfrak{f}(\eta), \hat{\vartheta}(\eta,1) = \vartheta(\eta), \hat{\Phi}(\eta,1) = \Phi(\eta) \tag{27}$$

As r moves from 0 to 1, $\hat{\mathfrak{f}}(\eta,r), \hat{\vartheta}(\eta,r) and \hat{\Phi}(\eta,r)$ varies from the initial approximation $\not{f}_0(\eta)$, $\vartheta_0(\eta)$, $\Phi_0(\eta)$ to exact solution $\mathfrak{f}(\eta)$, $\vartheta(\eta)$, $\Phi(\eta)$ respectively. Expanding $\hat{\mathfrak{f}}(\eta,r)$, $\hat{\vartheta}(\eta,r)$ and $\hat{\Phi}(\eta,r)$ by using Taylor's theorem with respect to r and then using Eqs. (23)–(25). One can write the above profiles in the form

$$\hat{\mathfrak{f}}(\eta,r) = \mathfrak{f}_0(\eta) + \sum_{q=1}^{\infty}\mathfrak{f}_q(\eta)r^q,\ \ \mathfrak{f}_q(\eta) = \frac{1}{q!}\left.\frac{\partial^q\hat{\mathfrak{f}}(\eta,r)}{\partial r^q}\right|_{r=0} \tag{28}$$

$$\hat{\vartheta}(\eta,r) = \vartheta_0(\eta) + \sum_{q=1}^{\infty}\vartheta_q(\eta)r^q,\ \ \vartheta_q(\eta) = \frac{1}{q!}\left.\frac{\partial^q\hat{\vartheta}(\eta,r)}{\partial r^q}\right|_{r=0} \tag{29}$$

$$\hat{\Phi}(\eta,r) = \Phi_0(\eta) + \sum_{q=1}^{\infty}\Phi_q(\eta)r^q,\ \ \Phi_q(\eta) = \frac{1}{q!}\left.\frac{\partial^q\hat{\Phi}(\eta,r)}{\partial r^q}\right|_{r=0} \tag{30}$$

Here $\mathfrak{f}_q(\eta), \vartheta_q(\eta) and \Phi_q(\eta)$ are called the qth-order deformation derivative. Now convergence at $r = 1$ can be shown for the above series as auxiliary function, initial guess, the auxiliary parameter and the auxiliary function be selected in good way. After that, we have

$$\mathfrak{f}(\eta) = \mathfrak{f}_0(\eta) + \sum_{q=1}^{\infty}\mathfrak{f}_q(\eta) \tag{31}$$

$$\vartheta(\eta) = \vartheta_0(\eta) + \sum_{q=1}^{\infty}\vartheta_q(\eta) \tag{32}$$

$$\Phi(\eta) = \Phi_0(\eta) + \sum_{q=1}^{\infty}\Phi_q(\eta) \tag{33}$$

3.2 Higher-order deformation equations

For Eqs. (31)–(33), define the vectors

$$\vec{\mathfrak{f}}_N(\eta) = \{\mathfrak{f}_0(\eta), \mathfrak{f}_1(\eta), \mathfrak{f}_2(\eta), \ldots, \mathfrak{f}_N(\eta)\} \tag{34}$$

$$\vec{\vartheta}_N(\eta) = \{\vartheta_0(\eta), \vartheta_1(\eta), \vartheta_2(\eta), \ldots, \vartheta_N(\eta)\} \tag{35}$$

$$\vec{\Phi}_N(\eta) = \{\Phi_0(\eta), \Phi_1(\eta), \Phi_2(\eta), \ldots, \Phi_N(\eta)\} \tag{36}$$

After differentiating the Eqs. (18)–(20) 'q' times with respect to r, dividing by $q!$ and set $r = 0$. The qth order deformation equations are

$$\mathcal{L}[\mathfrak{f}_q(\eta,r) - \chi_q\mathfrak{f}_{q-1}(\eta)] = \hbar_{\mathfrak{f}}\mathcal{H}(\eta)R_q(\vec{\mathfrak{f}}_{q-1}(\eta)) \tag{37}$$

$$\mathcal{L}[\vartheta_q(\eta,r) - \chi_q\vartheta_{q-1}(\eta)] = \hbar_{\vartheta}\mathcal{H}^*(\eta)R_q(\vec{\vartheta}_{q-1}(\eta)) \tag{38}$$

$$\mathcal{L}[\Phi_q(\eta,r) - \chi_q\Phi_{q-1}(\eta)] = \hbar_{\Phi}\mathcal{H}^{\#}(\eta)R_q(\vec{\Phi}_{q-1}(\eta)) \tag{39}$$

with boundary conditions

$$\mathfrak{f}_q(0) = \mathfrak{f}_q^{(1)}(0) = \mathfrak{f}_q^{(1)}(\infty) = 0, \vartheta_q(0) = \vartheta_q(\infty) = 0, \\ \Phi_q(0) = \Phi_q(\infty) = 0 \tag{40}$$

where

$$R_q(\mathfrak{f}_{q-1}(\eta)) = \frac{1}{(q-1)!}\left.\frac{\partial^{q-1}\mathcal{N}(\hat{\mathfrak{f}}(\eta,r))}{\partial r^{q-1}}\right|_{r=0} \tag{41}$$

$$R_q(\vartheta_{q-1}(\eta)) = \frac{1}{(q-1)!}\left.\frac{\partial^{q-1}\mathcal{N}(\hat{\vartheta}(\eta,r))}{\partial r^{q-1}}\right|_{r=0} \tag{42}$$

$$R_q(\Phi_{q-1}(\eta)) = \frac{1}{(q-1)!}\left.\frac{\partial^{q-1}\mathcal{N}(\Phi(\eta,r))}{\partial r^{q-1}}\right|_{r=0} \tag{43}$$

$$\chi_q = \begin{cases} 0, & q \leqslant 1 \\ 1, & q > 1 \end{cases} \tag{44}$$

Eqs. (41)–(44) further implies that

$$R_q^{\mathfrak{f}}(\eta) = \left(1 + \frac{1}{\beta}\right)\mathfrak{f}_{q-1}^{(3)}(\eta) + \sum_{K=0}^{q-1}\{\mathfrak{f}_{q-k-1}(\eta)\mathfrak{f}_k^{(2)}(\eta) - \mathfrak{f}_{q-k-1}^{(1)}\mathfrak{f}_k^{(1)}(\eta)\} \\ - A\mathfrak{f}_{q-1}^{(1)}(\eta) - \frac{A}{2}\eta\mathfrak{f}_{q-1}^{(2)}(\eta) + (\mathrm{A}+1)(1-\boldsymbol{\chi_q}) \tag{45}$$

$$R_q^{\vartheta}(\eta) = \vartheta_{q-1}^{(2)}(\eta) + \Pr\sum_{K=0}^{q-1}\{\mathfrak{f}_{q-k-1}(\eta)\vartheta_k^{(1)}(\eta) - \vartheta_{q-k-1}(\eta)\mathfrak{f}_k^{(1)}(\eta)\} \\ - APr\{\vartheta_{q-1}(\eta) + \frac{\eta}{2}\vartheta_{q-1}^{(1)}(\eta)\} \tag{46}$$

$$R_q^{\Phi}(\eta) = \Phi_{q-1}^{(2)}(\eta) + \mathrm{Sc}\{\sum_{K=0}^{q-1}\mathfrak{f}_{q-k-1}(\eta)\Phi_k^{(1)}(\eta) - A(\frac{\eta}{2}\Phi_{q-1}^{(1)}(\eta) \\ + \beta^*\Phi_{q-1}(\eta) \tag{47}$$

The symbolic software MATHEMATICA is used to solve the system of homogeneous linear equations (37)–(40) up-to some order of approximations and then found that it can be written as an infinite series of the form

$$\mathfrak{f}(\eta) = \lim_{M\to\infty}\sum_{q=0}^{M}\mathfrak{f}_q(\eta) \tag{48}$$

$$\vartheta(\eta) = \lim_{M\to\infty}\sum_{q=0}^{M}\vartheta_q(\eta) \tag{49}$$

$$\Phi(\eta) = \lim_{M\to\infty}\sum_{q=0}^{M}\Phi_q(\eta) \tag{50}$$

Results and discussion

The successive iterations of velocity, temperature and concentration after 1st iteration are as follows

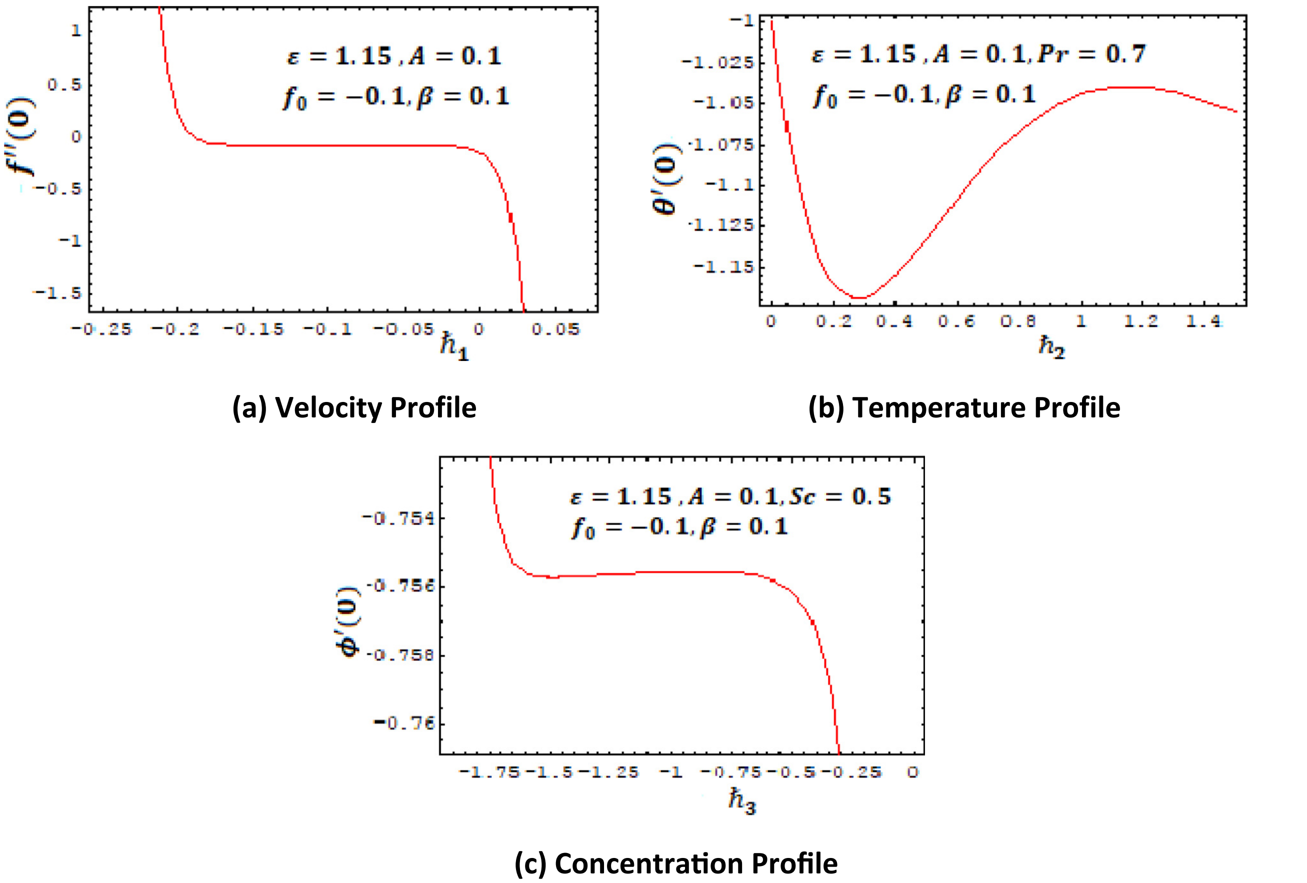

Fig. 2. $\hbar$-curves of (a) Velocity Profile; (b) Temperature Profile; (c) Concentration Profile.

Table 1
Convergence of HAM Solution.

$A = 0.1, \in = 1.15, \beta = 0.1$	$f_0 = -0.1, Pr = 0.7, Sc = 0.5, \beta^* = 1$		
Order of Approximation	$-\mathfrak{f}^{(2)}(0)$	$-\vartheta^{(1)}(0)$	$-\mathbf{\Phi}^{(1)}(0)$
1	0.144800	1.235499	0.780000
10	0.187349	1.201256	0.775433
15	0.192995	1.165346	0.765432
20	0.198728	1.050355	0.755345
25	0.198728	1.050355	0.755345
30	0.198728	1.050355	0.755345
35	0.198728	1.050355	0.755345
40	0.198728	1.050355	0.755345

$$
\begin{aligned}
\mathfrak{f}_1(\eta) = {} & \mathrm{f}_0 - \frac{\mathrm{h1}}{4} + \frac{5A\mathrm{h1}}{8} - \frac{1}{2}\mathrm{e}^{-2\eta}\mathrm{h1} - \frac{1}{2}A\mathrm{e}^{-2\eta}\mathrm{h1} + \frac{3\mathrm{e}^{-\eta}\mathrm{h1}}{4} \\
& - \frac{1}{8}A\mathrm{e}^{-\eta}\mathrm{h1} - \frac{\mathrm{f}_0\mathrm{h1}}{4} - \frac{1}{4}\mathrm{e}^{-2\eta}\mathrm{f}_0\mathrm{h1} + \frac{1}{2}\mathrm{e}^{-\eta}\mathrm{f}_0\mathrm{h1} + \frac{\mathrm{h1}}{4\beta} + \frac{\mathrm{e}^{-2\eta}\mathrm{h1}}{4\beta} \\
& - \frac{\mathrm{e}^{-\eta}\mathrm{h1}}{2\beta} + (-1 + \mathrm{e}^{-\eta})(1-\gamma) + \frac{3A\mathrm{h1}\gamma}{8} + \frac{1}{4}\mathrm{e}^{-2\eta}\mathrm{h1}\gamma \\
& + \frac{1}{2}A\mathrm{e}^{-2\eta}\mathrm{h1}\gamma - \frac{1}{4}\mathrm{e}^{-\eta}\mathrm{h1}\gamma - \frac{7}{8}A\mathrm{e}^{-\eta}\mathrm{h1}\gamma + \frac{\mathrm{f}_0\mathrm{h1}\gamma}{4} \\
& + \frac{1}{4}\mathrm{e}^{-2\eta}\mathrm{f}_0\mathrm{h1}\gamma - \frac{1}{2}\mathrm{e}^{-\eta}\mathrm{f}_0\mathrm{h1}\gamma - \frac{\mathrm{h1}\gamma}{4\beta} - \frac{\mathrm{e}^{-2\eta}\mathrm{h1}\gamma}{4\beta} + \frac{\mathrm{e}^{-\eta}\mathrm{h1}\gamma}{2\beta} \\
& + \frac{\mathrm{h1}\gamma^2}{4} + \frac{1}{4}\mathrm{e}^{-2\eta}\mathrm{h1}\gamma^2 - \frac{1}{2}\mathrm{e}^{-\eta}\mathrm{h1}\gamma^2 + \eta - \frac{1}{4}\mathrm{e}^{-2\eta}\mathrm{h1}\eta \\
& - \frac{1}{8}A\mathrm{e}^{-2\eta}\mathrm{h1}\eta - A\mathrm{e}^{-\eta}\mathrm{h1}\eta + \frac{1}{4}\mathrm{e}^{-2\eta}\mathrm{h1}\gamma\eta + \frac{1}{8}A\mathrm{e}^{-2\eta}\mathrm{h1}\gamma\eta \\
& - \frac{1}{4}A\mathrm{e}^{-\eta}\mathrm{h1}\eta^2
\end{aligned}
$$

Table 2
Values of $\mathfrak{f}''(0)$for multiple values of γ for $\beta = \infty$ (Newtonian fluid case) when A = 0.

γ	Present Study	K-Bhattacharyya [4]	Wang [15]	M. Suali [36]
0	1.2325877	1.2325878	1.2325888	
0.1	1.1465512	1.1465608	1.1465601	1.146561
0.2	1.0511291	1.0511299	1.0511312	1.051130
0.5	0.7132888	0.7132951	0.7133023	
1	0	0	0	
3	-4.2765455			-4.276545

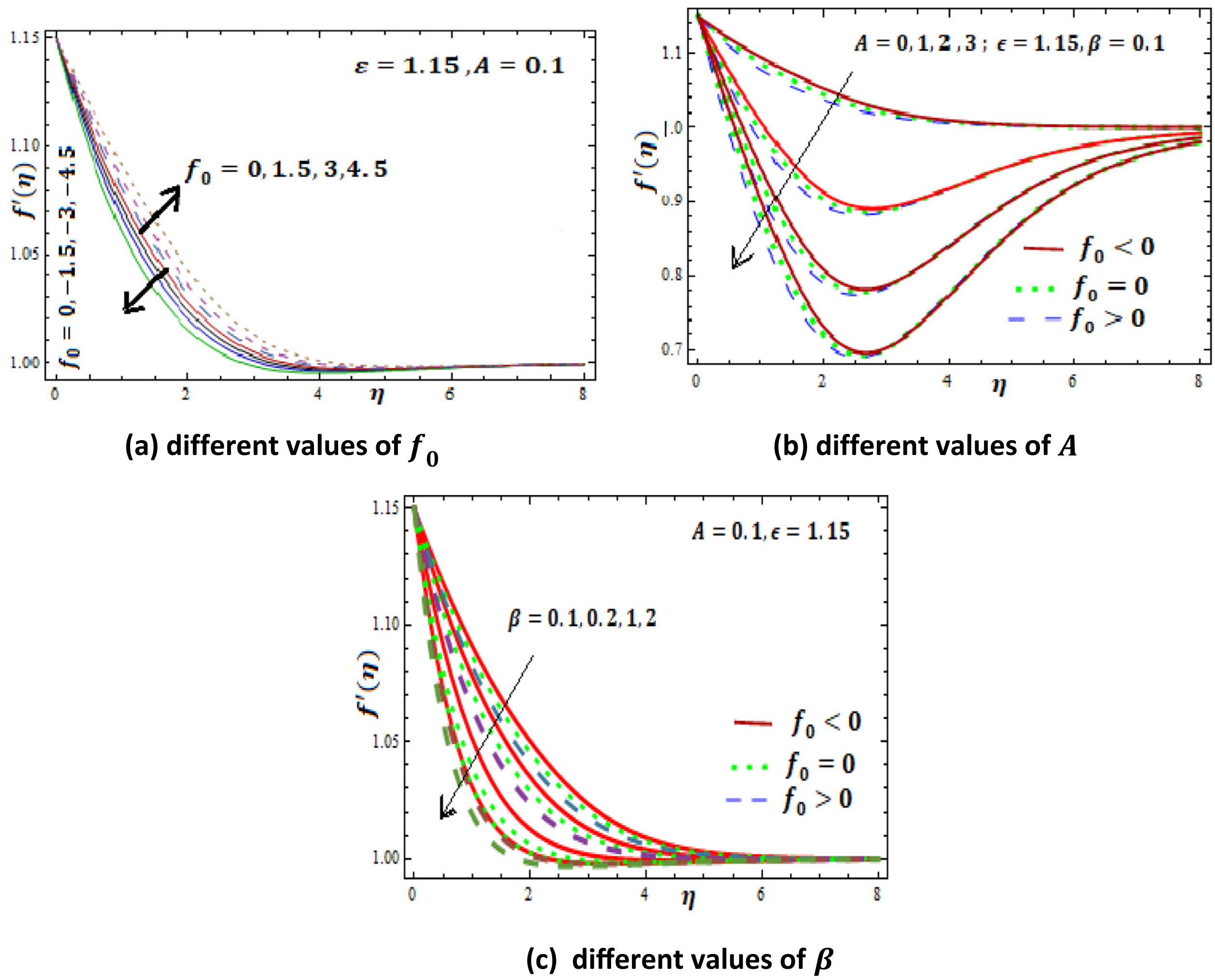

Fig. 3. Velocity Profile$f'(\eta)$ for (a) different values of f_0; (b) different values of A.

$$\vartheta_1(\eta) = e^{-\eta} - \frac{1}{4}e^{-2\eta}h2 + \frac{e^{-\eta}h2}{4} + \frac{1}{2}e^{-2\eta}h2Pr - \frac{1}{2}e^{-\eta}h2Pr + \frac{1}{4}e^{-2\eta}f_0h2Pr - \frac{1}{4}e^{-\eta}f_0h2Pr + \frac{1}{4}e^{-2\eta}h2Pr\gamma - \frac{1}{4}e^{-\eta}h2Pr\gamma + \frac{1}{4}e^{-2\eta}h2Pr\eta - \frac{1}{8}Ae^{-2\eta}h2Pr\eta$$

$$\Phi_1(\eta) = e^{-\eta} + \frac{1}{2}e^{-2\eta}h3 - \frac{e^{-\eta}h3}{2} - \frac{1}{6}e^{-3\eta}h3Sc - \frac{1}{4}e^{-2\eta}h3Sc + \frac{3}{8}Ae^{-2\eta}h3Sc + \frac{5}{12}e^{-\eta}h3Sc - \frac{3}{8}Ae^{-\eta}h3Sc - \frac{1}{2}e^{-2\eta}f_0h3Sc + \frac{1}{2}e^{-\eta}f_0h3Sc - \frac{1}{2}e^{-2\eta}h3Sc\beta^* + \frac{1}{2}e^{-\eta}h3Sc\beta^* + \frac{1}{6}e^{-3\eta}h3Sc\gamma - \frac{1}{2}e^{-2\eta}h3Sc\gamma + \frac{1}{3}e^{-\eta}h3Sc\gamma - \frac{1}{2}e^{-2\eta}h3Sc\eta + \frac{1}{4}Ae^{-2\eta}h3Sc\eta$$

The convergence of the above-mentioned series (48)–(50) firmly based on the control parameter of convergence $\hbar_f = h1, \hbar_\vartheta = h2, \hbar_\Phi = h3$where the admissible range observed from Fig. 2 of 22nd order approximation drawn below is $-0.18 \leqslant \hbar_f \leqslant 0.01$, $1.05 \leqslant \hbar_\vartheta \leqslant 1.25$ and $-1.5 \leqslant \hbar_\Phi \leqslant -0.5$. The numerical calculations of our problem with the help of square residual error (For details, see [41]) tell that velocity field of series no (48) converges in the whole region of η for $\hbar_f = -0.1303$. In the same way, series no (49) and (50) converges at $\hbar_\vartheta = 1.112$ and $\hbar_\Phi = -1.1$. Table 1 shows the convergence of HAM solution up to different order of approximation.

In the present article, we are directed to discuss the effects of Casson fluid in the unsteady model of the stretching sheet with suction/injection mass transfer affects in the presence of heat, mass transfer and chemical reaction. The involvement of unique solution occurred due to stretching sheet with velocity ratio has already be explained by [36]. In this current study, the similar unique solution will be discussed with the presence of non-Newtonian Casson fluid and mass transfer analysis. And to validate the HAM technique, values of $f''(0)$ for $\beta = \infty$ in Table 2 has been found in reasonable manner with already published research work.

Influence of important parameters on dimension-free velocity, temperature and concentration profiles are discussed in detail in Figs. 3–6. Fig. 3a exhibits remarkably that mass suction increases the velocity profile of Casson fluid but reverse outcomes are seen in mass injection. It informs that there is no reverse flow in the boundary layer as rate of change in $\boldsymbol{f}(\eta)$ is nowhere negative. Fig. 3b elaborates the different cases of wall mass transfer against several values of unsteadiness parameter **A**. It declares that boundary layer thickness of Casson fluid flow decreases overall in all the discussed cases as the values of **A** increases. Important to note that, mass injection brings major effects where velocity profile decreases slowly as compared to other cases. But as $\eta > 2.9713$

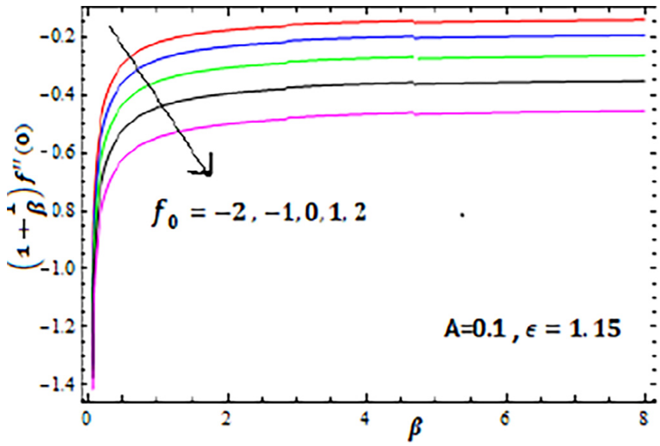

Fig. 4. Variation of skin friction for several values of β (a) different values of f_0; (b) different values of A; (c) different values of β.

i.e. fluid moving away from the stagnation point, velocity profile converges to one. In Fig. 3c, velocity profile $f'(\eta)$decline for each Casson parameter β but increasing the value of β also decreases the velocity profile $f'(\eta)$and momentum boundary layer thickness because raise the volume of plastic dynamic viscosity always slows down the fluid motion due to its resistive nature. Moreover, it is evident from the above figures that while increasing the value of β, velocity of fluid is greater in mass injection as compared to mass suction. The physical quantity of concern which is proportional to the results of $(1+\frac{1}{\beta})f''(0)$is the wall skin friction coefficient which has many important applications in engineering field. Fig. 4 describes that wall skin friction coefficient increases for several values of β either wall mass injection/suction is involved or not. Larger the injection value increases the wall skin friction. Overall it decreases from mass injection to suction for values of β. It informs that on the fluid, medium exerts a dragging force due to the negative value of skin friction $(1+\frac{1}{\beta})f''(0)$. Table 3 present the detailed picture of skin friction coefficient. It reflects the same that as the value of Casson parameter increases, the skin friction coefficient also increases whether wall mass transfer is through injection or suction. But suction effects are more dominant to injection effects. Higher the suction effects increase the skin friction coefficient absolutely. Fig. 5 gives the detail picture of thermal boundary layer. Larger the value of non-Newtonian parameter raises the thermal boundary layer thickness in all cases of wall mass transfer, see Fig. 5a. It is quite understandable that Casson parameter always raises the thermal thickness of boundary layer. But overall thermal boundary layer profile decreases for each β.

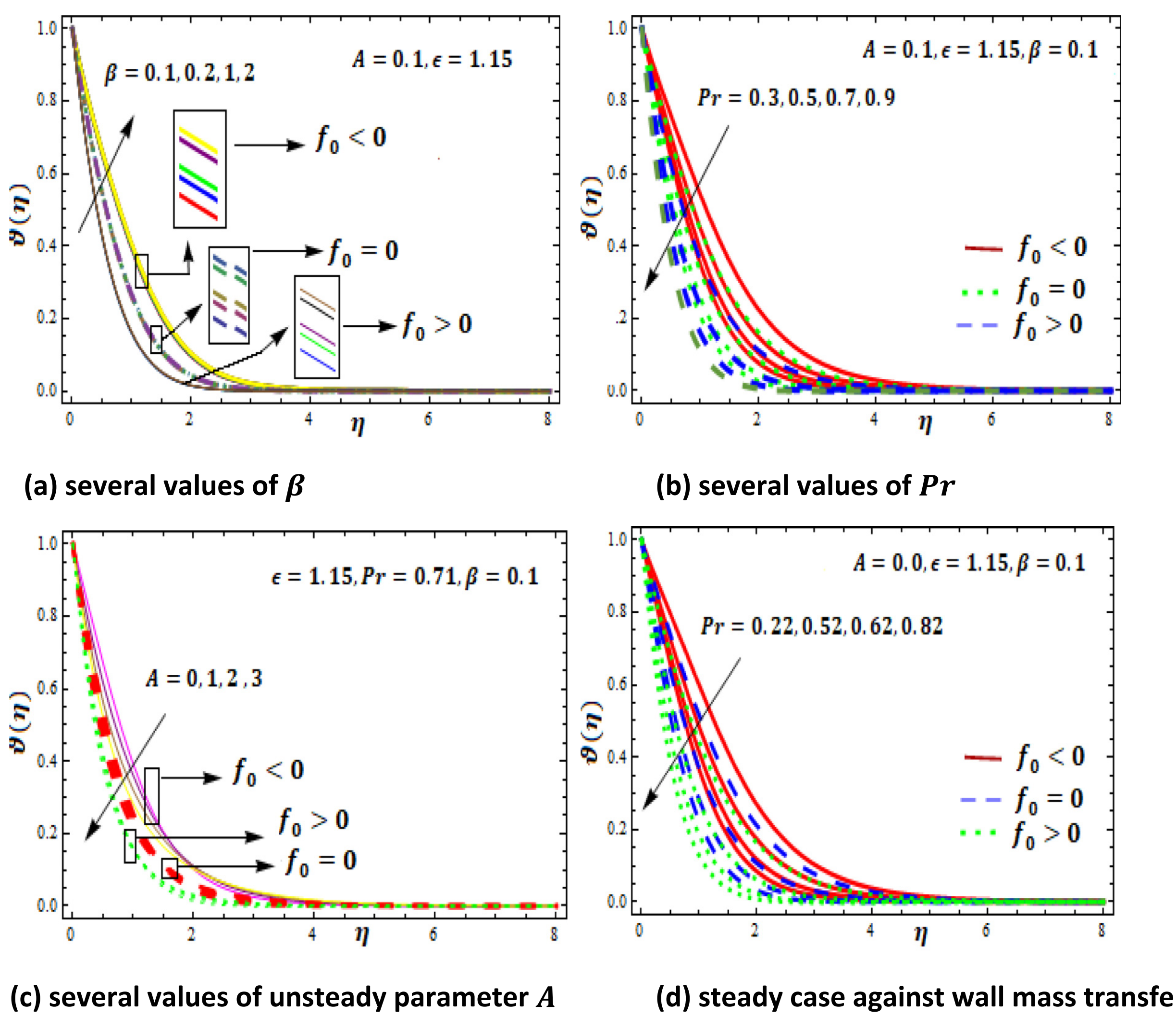

Fig. 5. Temperature influence $\vartheta(\eta)$ for (a) several values of β; (b) several values of Pr; (c) several values of unsteady parameter A; (d) steady case against wall mass transfer.

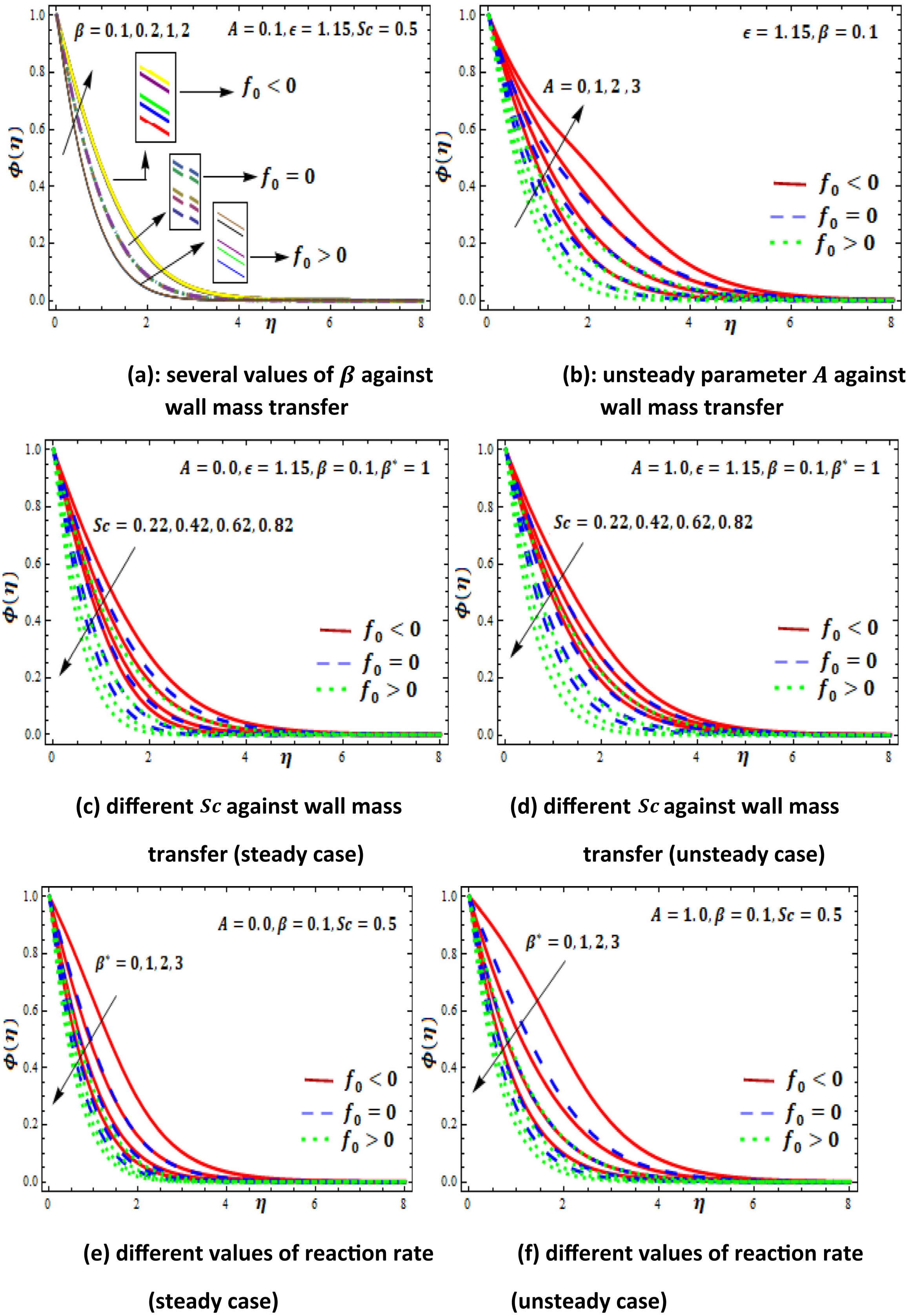

Fig. 6. Concentration influence $\Phi(\eta)$ for (a): several values of β against wall mass transfer; (b): unsteady parameter *A* against wall mass transfer; (c) different *Sc* against wall mass transfer (steady case); (d) different *Sc* against wall mass transfer (unsteady case); (e) different values of reaction rate (steady case); (f) different values of reaction rate (unsteady case).

Table 3
Skin Friction Coefficient for 30th approximation.

A	Pr	Sc	f_0	β	$\left(1+\frac{1}{\beta}\right)f''(0)$	A	Pr	Sc	f_0	β	$(1+\frac{1}{\beta})f''(0)$
0.01	0.7	0.5	−2	0.1	−0.6950611					2	−0.233717
				0.2	−0.4702941					5	−0.202921
				0.3	−0.3789356					100	−0.181581
				0.4	−0.3276822	0.01	0.7	0.5	0	0.1	−0.844791
				0.5	−0.2944311					0.2	−0.616445
				1	−0.2200264					0.3	−0.522311
				2	−0.1773332					0.4	−0.468882
				5	−0.1493234					0.5	−0.433887
				100	−0.1304363					1	−0.354163
0.01	0.7	0.5	−1	0.1	−0.766832					2	−0.306625
				0.2	−0.538977					5	−0.273663
				0.3	−0.445381					100	−0.249972
				0.4	−0.392425	0.01	0.7	0.5	1	0.1	−0.928881
				0.5	−0.357834					0.2	−0.702857
				1	−0.279534					0.3	−0.609585
0.01	0.7	0.5	2	0.1	−1.01896	0.01	0.7	0.5	2	1	−0.547339
				0.2	−0.797064					2	−0.500528
				0.3	−0.706688					5	−0.465112
				0.4	−0.655829					100	−0.437102
				0.5	−0.622715						

Table 4
Local Nusselt Number for 30th approximation.

A	Pr	Sc	f_0	β	$-\vartheta'(0)$	A	Pr	Sc	f_0	β	$-\vartheta'(0)$
0.0	0.22	0.5	−1	0.1	0.475759	0.1	0.62				1.449211
				0.2	0.473433	0.01	0.7	0.5	−1	0.1	0.811811
				0.3	0.471931				−0.5		0.943988
				1	0.468028				0.0		1.116771
				2	0.466652				0.5		1.325351
	0.71			0.1	0.696526				1		1.563051
				0.2	0.694523				−1	0.2	0.809550
				0.3	0.692853				−0.5		0.941065
				1	0.687376				0.0		1.113341
	0.71		0	0.1	1.08272				0.5		1.321580
				0.2	1.07915				−1	0.3	0.803366
				0.3	1.07665				−0.5		0.939343
				1	1.06943				0.0		1.111201
			1	0.1	1.57582				0.5		1.319160
				0.2	1.57171				−1	1	0.805274
				0.3	1.56888				−0.5		0.934526
				1	1.56095				0.0		1.105041
	0.3		−1	0.1	0.53689				0.5		1.312054
	0.5				0.635132				−1	0.1	0.811811
	0.7				0.694118					0.2	0.809550
	0.3		0		0.692067					0.3	0.808366
	0.5				0.900031				0	0.1	1.116770
	0.3		1		0.885276					0.2	1.113340
	0.5				1.239411				1	0.1	1.563051
	0.7				1.560421					0.2	1.559100
0.1	0.22		−1	0.1	0.489469	0.1	0.22		−1	0.1	0.601756
	0.42				0.622116		0.42				0.838272
	1				0.786081		1				1.327813
	1.22				0.823821		1.22				1.480883
0.1	0.22		1		0.737743	0.1	0.82		1		1.757031
	0.42				1.115330		1				2.016121

Further Fig. 5b, d shows the temperature's influence for the multiple values of Prandtl number. It smokes out that increasing the value of Prandtl number lowers down the temperature profile. Prandtl number always regulate the relative thickness of the momentum and the thermal boundary layer. For small Prandtl number, where the thermal boundary layer is bigger than the momentum boundary layer, heat diffuse quickly. Hence Prandtl number can be used to increases the cooling rate of conducting flows. Moreover, the thermal boundary layer thickness declines after enlarging the Prandtl number as best depicted in Fig. 5b,5d. Observation is that mass blowing process raises the temperature as compared to other mass transfer analysis for any value of unsteady parameter **A**. Fig. 5c represent the different sections of thermal reading against the different unsteady parameters for all cases of wall mass transfer. Dotted curves where no mass transfer involves, 1st part represent that as fluid closest to the stagnation point, temperature profile decreases but in 2nd part it increases either the model is steady or unsteady. Fig. 6a-6f shows the concentration influence for different parameters of given model. Fig. 6a demonstrate that profile decreases for each β but increasing the value of β also raises the concentration profile. Fig. 6b shows that concentration profile also increases but suction has lower concentration overall as compared to other cases. Fig. 6c–d represent that increasing the value of Schmidt number lowers down the concentration boundary layer. It informs that heavier species attempt to hold back the concentration level. Also, these diagrams declare

Table 5
Sherwood Number for 30th approximation.

A	Sc	f_0	β	β^*	$-\Phi'(0)$	A	Sc	f_0	β	β^*	$-\Phi'(0)$
0.01	0.5	−1	0.1	1	0.648741	0	0.5	0	0.1	1	0.903517
		0.5			0.768253	1					0.807225
		0			0.904325	2					0.712304
		0.5			1.055761	3					0.623383
		1			1.220911	0	0.5	1	0.1	1	1.220711
		−1	0.2		0.647638	1					1.115181
		0.5			0.766938	2					1.003771
		0			0.902825	3					0.889873
		0.5			1.054177	0	0.22	−1	0.1		0.487451
		1			1.219171		0.42				0.611294
		−1	0.3		0.646987		0.62				0.695823
		0.5			0.766146		0.82				0.756929
		0			0.901904	0	0.5	−1	0.1	0	0.311741
		0.5			1.053091					1	0.648705
		1			1.218061					2	0.894944
		−1	1		0.645352					3	1.096641
		0.5			0.764102		0.5	0	0.1	0	0.581597
		0			0.899469					1	0.903517
		0.5			1.050311					2	1.143561
		1			1.215001					3	1.342481
		−1	0.1		0.648741		0.5	1	0.1	0	0.935216
			0.2		0.647638					1	1.220710
			0.3		0.646987					2	1.443611
			1		0.6445352					3	1.633041
			2		0.644742	0.1	0.5	−1	0.1	0	0.299116
		0	0.1		0.904325					1	0.640719
			0.2		0.902825					2	0.888979
			0.3		0.901904					3	1.091741
			1		0.899469	0		−1	0.1	0	0.311741
			2		0.898521	1					0.187893
		1	0.1		1.220911	2					0.075044
			0.2		1.219170	0		0	0.1		0.581597
			0.3		1.218066	1					0.425406
			1		1.215013	2					0.264961
			2		1.213771	0		1	0.1		0.935216
0		−1	0.1		0.648705	1					0.767266
1					0.571258	2					0.578751
2					0.501559						
3					0.443695						

that concentration boundary layer decreases overall but higher concentration is observed in unsteady case as compared to time independent case. Fig. 6e, f informs about the influence of chemical reaction parameter. It is the observation that rise in the value of reaction rate parameter releases heat energy and it declines the concentration boundary layer of Casson fluid. It reveals that higher the level of impurities lower down the concentration profile. Table 4 depicts the influence of heat transfer coefficients on different parameters. It shows that N_u decreases by enhancing the value of Casson parameter but higher the Prandtl value increases the rate of heat transfer in all the cases of different wall mass transfer parameters. Once again, rate of heat transfer is greater in magnitude in suction effects as compared to mass blowing or no mass transfer. Most important is, rate of heat transfer is greater under the influence of unsteady model as compared to steady model. Table 5 depicts the influence of mass transfer coefficients on different parameters. Sherwood number decreases by enhancing the value of Casson parameter but increases by increasing the value of wall mass transfer $f_0$but most important is, rate of mass transfer increases as reaction rate parameter enhances but decline is observed for all the values of f_0 but individual profiles of Sherwood number decreases while increasing the value of unsteady parameter A.

Conclusion

The present study deals the numerical solution of the influence of heat and mass transfer of an unsteady Casson fluid model with wall mass transfer past a stretching sheet. Some key findings are discussed below. Enlarge the value of unsteady parameter **A**, from wall mass injection to suction, velocity profile attains absolute minima near the stagnation point. Time dependent phenomena reduce the boundary layer thickness as compared to steady effects. Increases the Casson parameter decrease the velocity influence and concentration profile but enhances the thermal boundary layer. Larger the mass suction rate at any specified value of β shows dominancy that it reduces the thermal boundary and concentration profile.

Appendix A. Supplementary data

Supplementary data associated with this article can be found, in the online version, at https://doi.org/10.1016/j.rinp.2017.12.080.

References

[1] Fredrickson AG. Principles and applications of rheology. Englewood Cliffs: N J Prentice Hall; 1964.
[2] Mustafa M, Hayat T, Pop I, Aziz A. Unsteady boundary layer flow of a Casson fluid due to an impulsively started moving flat. Heat Trans Asian Res 2011;40:563–76.
[3] Liao SJ. On the analytic solutions of magnetohydrodynamic flows of non-Newtonian fluids over a stretching sheet. J Fluid Mech 2003;488:189–212.
[4] Bhattacharyya K. Boundary layer stagnation point flow of Casson fluid and heat transfer towards a shrinking/stretching sheet. Front Heat Mass Trans 2013;4. https://doi.org/10.5098/hmt. v4.2.3003.
[5] Kumaran G, Sandeep N, Ali ME. Computational analysis of magnetohydrodynamic Casson and Maxwell flows over a stretching sheet with cross diffusion. Results Phys 2017;7:147–55.

[6] Pramanik S. Casson fluid and heat transfer past an exponentially porous stretching surface in the presence of thermal radiation. Ain Shams Eng J 2014;5:205–12.
[7] Oyelakin IS, Mondal S, Sibanda P. Unsteady Casson nanofluid flow over a stretching sheet with thermal radiation, convective and slip boundary conditions. Alexandria Eng J 2016;55:1025–35.
[8] Mukhopadhyay S. Casson fluid and heat transfer over a nonlinearly stretching surface. Chin Phys B 2013;22. https://doi.org/10.1088/1674-1056/22/7/074701.
[9] Zheng L, Niu J, Zhang X, Ma L. Dual solutions for flow and radiative heat transfer of a micropolar fluid over stretching/shrinking sheet. Int J Heat Mass Trans 2012;55:7577–86.
[10] Pal D. Heat and mass transfer in stagnation point flow towards a stretching surface in the presence of buoyancy force and thermal radiation. An Int J Theor Appl Mech 2009;44:145–58.
[11] Mahapatra TR, Dholey S, Gupta AS. Oblique stagnation point flow of an incompressible visco-elastic fluid towards a stretching sheet. Int J Nonlinear Mech 2007;42:484–99.
[12] Crane LJ. Flow past a stretching plate. Jape Math Phys (ZAMP) 1970;21:645–7.
[13] Chiam TC. Stagnation point flow towards a stretching plate. J Phys Soc Jap 1994;63:2443–4.
[14] Chiam TC. Heat transfer with variable conductivity in a stagnation-point flow towards a stretching sheet. Int Comm Heat Mass Trans 1996;23:239–48.
[15] Wang CY. Stagnation flow towards a shrinking sheet. Int J Nonlinearly Mech 2008;43(5):377–82.
[16] Sajid M, Javed T, Hayat T. MHD rotating flow of a viscous fluid over a stretching surface. Nonlinear Dyn 2008;51:259–65.
[17] Sajid M, Hayat T. The application of homotopy analysis method for MHD viscous flow due to a stretching surface. Chaos, Solitons Fractals 2009;39:1317–23.
[18] Sajid M, Hayat T. Influence of thermal radiation on the boundary layer flow due to an exponentially stretching sheet. Int Commun Heat Mass Trans 2008;35:347–56.
[19] Ishak A, Jafar K, Nazar R, Pop I. MHD stagnation point flow towards a stretching sheet. Physica A 2009;388:3377–83.
[20] Nadeem S, Hussain A, Khan M. HAM solutions for boundary layer flow in the region of the stagnation point towards a stretching sheet. Commun Nonlinear Sci Numer Simulat 2010;15:475–81.
[21] Gorder RAV, Vajravelu K. Hydromagnetic stagnation point flow of a second-grade fluid over a stretching sheet. Mech Res Commun 2010;37:113–8.
[22] Noor NFM, Awang Kechil S, Hashim I. Simple non-perturbative solution for MHD viscous flow due to a stretching sheet. Commun Nonlinear Sci Numer Simulat 2010;15:144–8.
[23] Rehman Abdul, Nadeem S, Malik MY. Stagnation flow of couple stress nanofluid over an exponentially stretching sheet through a porous medium. J Power Tech 2013;93(2):122–32.
[24] Bhattacharyya K. MHD Stagnation point flow of Casson fluid and heat transfer over a stretching sheet with thermal radiation. J Thermodyn 2013. https://doi.org/10.1155/2013/169674.
[25] Bhattacharyya K. Dual solutions in boundary layer stagnation-point flow and mass transfer with chemical reaction past a stretching/shrinking sheet. Int Commun Heat Mass Trans 2011;38:917–22.
[26] Bhattacharyya K, Hayat T, Alsaedi A. Analytic solutions for magneto hydrodynamics boundary layer flow of Casson fluid flow over a stretching/shrinking sheet with wall mass transfer. Chin Phys 2013;22:6.
[27] Shehzad SA, Hayat T, Qasim M, Asghar S. Effects of mass transfer on MHD flow of Casson fluid with chemical reaction and suction. Brazilian J Chem Eng 2013;30:187–95.
[28] Raju CSK, Sandeep N, Sugunamma V, Jayachandra M, Ramana Reddy JV. Heat and mass transfer in magnetohydrodynamic Casson fluid over an exponentially permeable stretching surface. Eng Sci Tech 2016;19:45–52.
[29] Ashraf MB, Hayat T, Alsaedi A. Mixed Convection flow of Casson Fluid over a stretching sheet with convective boundary conditions and Hall effects. Boundary Value Problems 2017. https://doi.org/10.1186/s13661-017-0869-7.
[30] Dehghan M, Abbaszadeh M. Proper orthogonal decomposition variational multiscale element free Galerkin (POD-VMEFG) meshless method for solving incompressible Navier-Stokes equation. Comput Methods App Mech Eng 2016;311:856–88.
[31] Dehghan M. An adaptive meshless local Petro-Glarkin method based on a posteriori error estimation for the boundary layer problems. App Numer Math 2017;111:181–96.
[32] Dehghan M, Abbaszadeh M. A finite element method for the numerical solution of Rayleigh-Stokes problem for a heated generalized second grade fluid with fractional derivatives. Eng Comput 2017;33:587–605.
[33] Tsai C. Homotopy method of fundamental solutions of certain nonlinear partial differential equations. Eng Anal Boundary Elem 2012;36:1226–34.
[34] Nakamura M, Sawada T. Numerical study on the flow of a non-Newtonian fluid through an axisymmetric stenosis. J Bio Mech Eng 1988;110(2):137–43.
[35] Fang T, Lee CF, Zhang J. The boundary layers of an unsteady incompressible stagnation point flow with mass transfer. Int J Nonlinear Mech 2011;46:942–8.
[36] Suali M, Nik Long NMA, Ariffin NM. Unsteady stagnation point flow and heat transfer over a stretching/shrinking sheet with suction or injection. J App Math 2012:12. https://doi.org/10.1155/2012/781845.
[37] Liao SJ. Beyond Perturbation: Introduction to Homotopy Analysis Method. Boca Raton: Chapman and Hall CRC Press; 2003.
[38] Dehghan M, Manafian J, Saadatmandi A. Solving nonlinear fractional partial differential equations using the homotopy analysis method. Numer Meth Partial Diff Eq 2010;26(2):448–79.
[39] Dehghan M, Salehi R. A seminumeric approach for solution of the eikonal partial differential equation and its applications. Numer Method Partial Diff Equ 2010;26(3):702–22.
[40] Heris JM, Dehghan M, Saadatmandi A. Application of semi-analytical methods for solving the Rosenau-Hyman equation arising in the pattern formation in liquid drops. Int J Numer Meth Heat Fluid Flow 2012;23(6):777–90.
[41] Liao SJ. On the homotopy analysis method for nonlinear problems. Appl Math Comput 2004;147:499–513.